Is the North Pacific Victoria Mode a Predictor of Winter Rainfall over South China?

QIAN ZOU,[a,b] RUIQIANG DING,[c] JIANPING LI,[d,e] YU-HENG TSENG,[f] ZHAOLU HOU,[d,e] TAO WEN,[g] AND KAI JI[h]

[a] *State Key Laboratory of Numerical Modeling for Atmospheric Sciences and Geophysical Fluid Dynamics (LASG), Institute of Atmospheric Physics, Chinese Academy of Sciences, Beijing, China;* [b] *College of Earth Sciences, University of Chinese Academy of Sciences, Beijing, China;* [c] *State Key Laboratory of Earth Surface Processes and Resource Ecology, Beijing Normal University, Beijing, China;* [d] *Frontiers Science Center for Deep Ocean Multispheres and Earth System (FDOMES)/Key Laboratory of Physical Oceanography/Institute for Advanced Ocean Studies, Ocean University of China, Qingdao, China;* [e] *Laboratory for Ocean Dynamics and Climate, Pilot Qingdao National Laboratory for Marine Science and Technology, Qingdao, China;* [f] *Institute of Oceanography, National Taiwan University, Taipei, Taiwan;* [g] *Plateau Atmosphere and Environment Key Laboratory of Sichuan Province, Chengdu University of Information Technology, Chengdu, China;* [h] *College of Atmospheric Sciences, Lanzhou University, Lanzhou, China*

(Manuscript received 20 October 2019, in final form 18 July 2020)

ABSTRACT: This study investigates the connection between the North Pacific Victoria mode (VM) during the boreal spring [February–April (FMA)] and the following boreal winter [January–March (JFM)] rainfall over South China (SC). The VM is defined as the second empirical orthogonal function mode (EOF2) of sea surface temperature (SST) anomalies (SSTAs) in the North Pacific poleward of 20°N. It is found that the boreal spring VM has a significant positive correlation with the following winter rainfall over SC. Analyses indicate that a strong positive VM during spring can induce El Niño during the following winter via an air–sea interaction, resulting in the generation of an anomalous anticyclone over the western North Pacific (WNPAC). The anomalous southwesterlies along the southeast coast of East Asia associated with the WNPAC favor an abundant supply of water vapor and anomalous ascending motion over SC. As a result, winter rainfall over SC increases. A linear regression model based on the VM shows that the VM can act as an effective predictor of winter rainfall over SC about 1 year in advance. It also has a higher prediction skill than ENSO in predicting winter rainfall over SC.

KEYWORDS: Atmosphere-ocean interaction; ENSO; Anticyclones; Rainfall; Climate prediction

1. Introduction

South China (SC; 22°–28°N, 108°–120°E) is an important region in China on account of its strong economy and developed agriculture. The strong variability of the precipitation over SC has often caused large agricultural and economic impacts (Huang et al. 2010; Zhang et al. 2015). For instance, heavy rainfall and snowfall occurred during January 2008, strongly damaging the transportation, electricity supply, and agriculture (Zhou et al. 2009). Therefore, it is necessary to understand the variability of the precipitation over SC and related physical processes.

The variability of precipitation over SC is affected by many factors (Chan et al. 2004; Mao et al. 2011; Zhou 2011; Chang et al. 2019; Li and Zhao 2019; Yi et al. 2019). The East Asian monsoon and El Niño–Southern Oscillation (ENSO) are two vital factors for the variability of precipitation over SC (Jia and Ge 2017; Gao et al. 2019). Chen et al. (2011) argued that during the establishment of the East Asian summer monsoon, water vapor is transported from the Indochina Peninsula and the South China Sea to SC. A sufficient supply of water vapor, together with frontal systems over SC, results in frequent severe convective precipitation during May–June (the mei-yu season) over SC. The effects of ENSO events on seasonal rainfall over eastern China have also been extensively studied (Wang et al. 2000; Wu et al. 2003; Xie et al. 2009; Zhang et al. 1996, 1999, 2017; Yuan and Yang 2020). For example, Lin and Lu (2009) suggested that after El Niño peaks, the precipitation is significantly changed in eastern China (significantly enhanced in the Yangtze River valley while suppressed in the Huaihe River and Yellow River valleys) in the following early summer, which is due to the impact of persistent ENSO-related warming in the tropical troposphere on the atmospheric circulation.

Previous research on rainfall over SC has mainly focused on summer (Chan and Zhou 2005; Zhou and Wang 2006; Duan et al. 2013; Yim et al. 2014), and winter rainfall has received less attention. In fact, statistics show that the winter rainfall accounts for about 15% of annual total rainfall (Li and Ma 2012), and there is an increasing trend in the proportion of winter precipitation over SC (Sui et al. 2013). Thus, studies on the variation and prediction of winter rainfall over SC become more meaningful. Studies showed that El Niño induces positive precipitation anomalies over SC during its mature phase (Wang et al. 2000; Zhang and Sumi 2002; Wu et al. 2003). During the El Niño winter, the anomalous suppressed convections produce an anomalous low-level western North Pacific (WNP) anticyclone (WNPAC), whose northwest flank helps to enhance water vapor transport from ocean to SC and results in more winter rainfall over SC (Wu et al. 2010; Duan et al. 2013; Lu et al. 2017; Wu et al. 2017; Zhang et al. 2017). The sea surface temperature (SST) anomalies (SSTAs) over the South China Sea are also an important factor for the variability of winter rainfall over SC. Positive South China Sea SSTAs will induce low-level southwesterly anomalies, transporting more moisture and favoring increased winter rainfall

Corresponding author: Dr. Ruiqiang Ding, drq@bnu.edu.cn

DOI: 10.1175/JCLI-D-19-0789.1

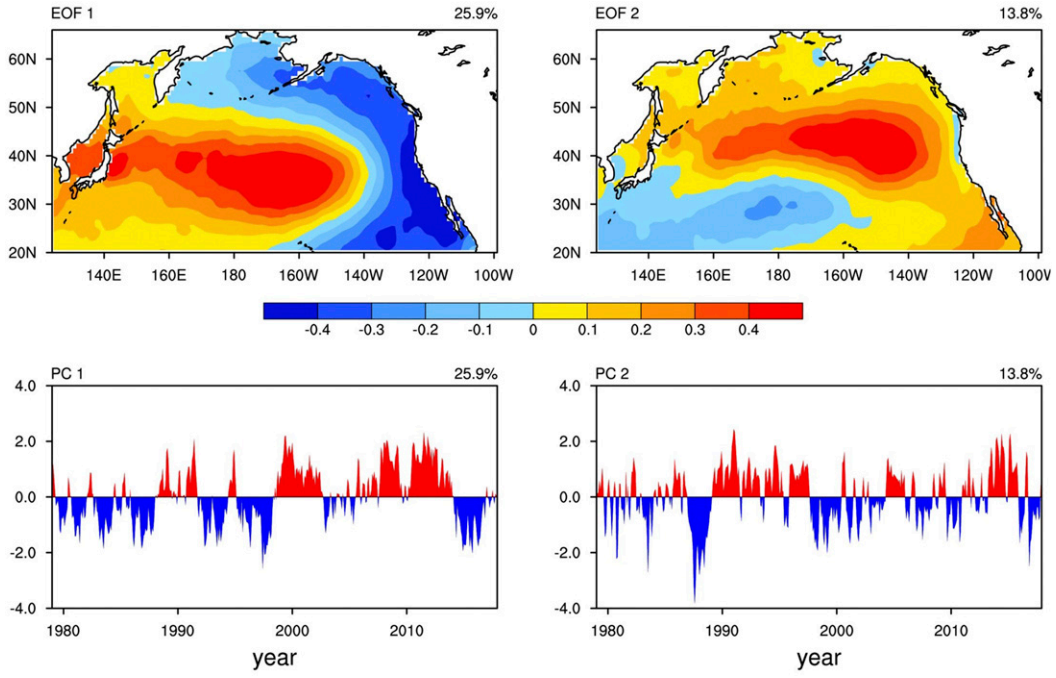

FIG. 1. (top) The two leading EOFs and (bottom) their corresponding PCs of the North Pacific (20.5°–65.5°N, 124.5°E–100.5°W) monthly SSTA field (with the monthly mean global average SSTA removed) for 1979–2017. Their variance contributions are given in the top-right corner of each panel.

over southern areas of China (Zhou et al. 2010; Zhang et al. 2015). The Indian Ocean SST also plays some roles in the winter precipitation over SC. When the SSTAs over eastern Indian Ocean are positive, local convection will deepen the India–Burma trough, enhancing the moisture transport from the Bay of Bengal and increasing the winter precipitation over SC (Peng 2012).

The above studies on winter rainfall over SC mainly pay attention to the impact of tropical signals such as ENSO and South China Sea SST. However, research showed that the extratropical signal can also exert an important influence on winter rainfall over SC (Chan and Zhou 2005; Gao et al. 2019). For instance, the winter rainfall over SC is significantly related to the intensity of the East Asian winter monsoon (Zhou 2011) through changing the atmospheric situation (Zhou and Wu 2010; Chen et al. 2014). When the East Asian winter monsoon is weak, southwesterly wind anomalies are dominant over the east flank of East Asia, which can favor anomalous moisture convergence and ascending motion, and then contribute to the increase in winter rainfall over SC (Zhou and Wu 2010; Zhou 2011; Ge et al. 2016). The North Atlantic Oscillation (NAO) and Arctic Oscillation (AO) are two vital teleconnections in the extratropical region over the Northern Hemisphere (Lou et al. 2017). Li and Sun (2015) argued that a phase transition of NAO was attributable to the heavy precipitation over SC during December 2013. During the decaying phase of medium positive NAO events, southerly winds are confined to the area south of 25°N, and precipitation is mainly limited in SC (Lou et al. 2017). During positive AO phases, the East Asian winter monsoon tends to be weaker (Wu and Wang 2002), which causes more rainfall over eastern China (Zhou and Wu 2010). Recently, a new extratropical signal known as the Victoria mode (VM) has received much attention. It is reported that the VM, an extratropical SST mode, can effectively influence tropical weather and climate variability, such as tropical cyclones (TCs) (Pu et al. 2019), ENSO (Ding et al. 2015b), the South China Sea summer monsoon (SCSSM) (Ding et al. 2018), and summer precipitation over the Pacific intertropical convergence zone (ITCZ) (Ding et al. 2015a). The VM exhibits prominent interannual variations, and it peaks in late winter and early spring [February–April (FMA)]. Given that the spring (here referring to FMA) VM influences subsequent ENSO events (Ding et al. 2015b), and ENSO can affect winter precipitation anomalies over SC (Zhang and Sumi 2002), it is natural to ask whether there exists a connection between the spring VM and the winter rainfall over SC. It is speculated that the VM exerts an influence on the winter rainfall over SC, and ENSO can act as a bridge for the VM's effects on winter rainfall over SC. Therefore, this study aims to analyze the effects of the spring VM on the following winter precipitation over SC and to determine the role of ENSO in this process. If our speculation is confirmed, the VM may act as a predictor of winter precipitation over SC about one year in advance.

In this paper, we investigate the relationship between the spring VM and the following winter rainfall over SC using observations and numerical simulations. The underlying mechanism is also elaborated. The remainder of this paper is organized as follows. Section 2 describes the datasets and

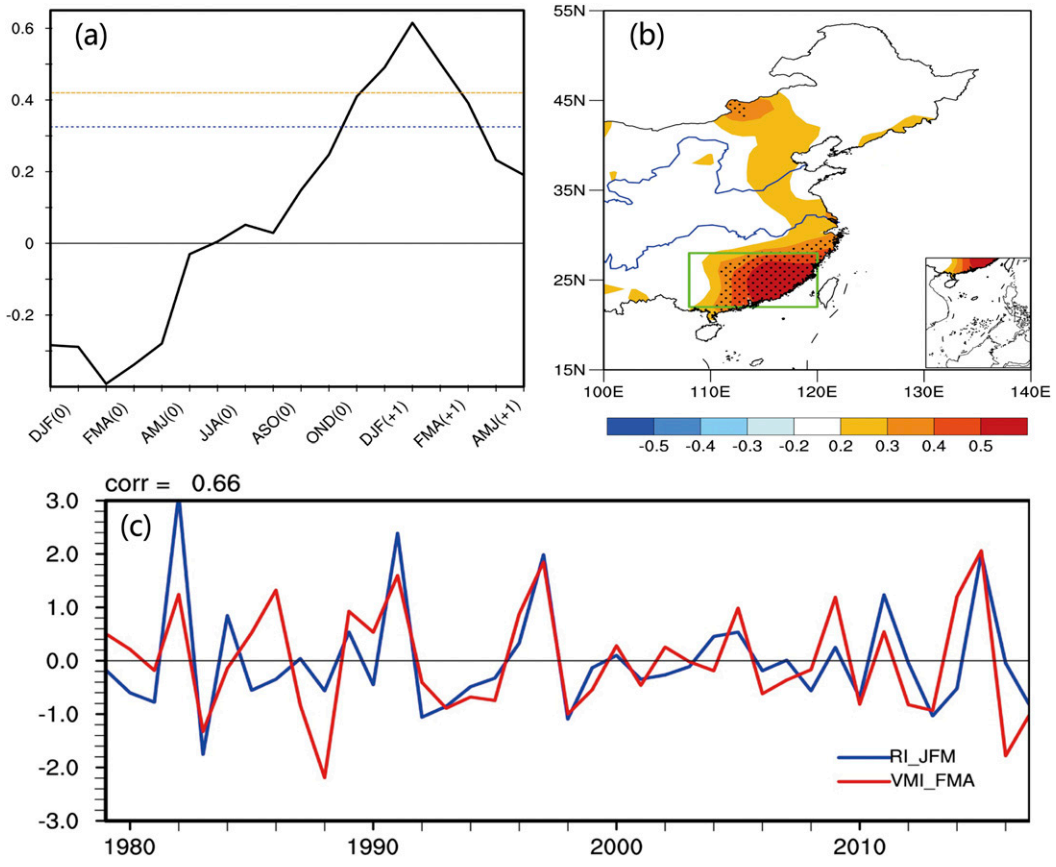

FIG. 2. (a) Lead–lag correlation coefficients between the FMA(0)-averaged VMI and overlapping 3-month averaged RI. The horizontal dashed lines show the 95% (blue) and 99% (yellow) confidence levels. (b) Correlation maps of the JFM(+1) rainfall anomalies in eastern China with FMA(0)-averaged VMI. Dots show correlations significant above the 95% confidence level. The green box indicates the SC area considered in this study (22°–28°N, 108°–120°E). (c) Time series of the FMA(0) VMI (red line) and the following JFM(+1)-averaged RI (RI_JFM) (blue line) for the period 1979–2017. Here and throughout, we denote the year in which the VM peaks in FMA as year 0 and the preceding and following years as year −1 and +1, respectively.

methods used. Section 3 establishes a relationship between the spring VM and winter rainfall over SC. Section 4 explores the possible physical mechanisms. A regression model using the VM to predict the winter rainfall over SC is established in section 5. Finally, section 6 provides a summary of our major findings.

2. Datasets and methodology

a. Observational data

Monthly rainfall data from 160 stations in China covering the period 1951–2018 are provided by the Chinese Meteorological Data Center. The atmospheric data are derived from the National Centers for Environmental Prediction–Department of Energy (NCEP–DOE) reanalysis version 2 (NCEP2) (1979–2018), on a horizontal resolution of 2.5° × 2.5° (Kanamitsu et al. 2002). The monthly SST data are from the Hadley Centre Sea Ice and Sea Surface Temperature dataset (HadISST) on a 1° × 1° spatial grid (Rayner et al. 2003). The variation of ENSO is represented by the Niño-3.4 index defined as the December–February (DJF) SST anomaly over the region 5°S–5°N, 170°–120°W, obtained from the NOAA Climate Prediction Center (https://www.esrl.noaa.gov/psd/data/climateindices/). We analyze the period 1979–2018, and choose the period 1981–2010 to define the climatology. The monthly anomalies are computed by removing the climatological monthly mean.

b. Numerical models

To further demonstrate the effects of the spring VM on the following winter rainfall over SC, coupled model sensitivity experiments were conducted. We used the Flexible Global Ocean–Atmosphere–Land System Model Grid-point version 2 (FGOALS-g2), which is developed by the State Key Laboratory of Numerical Modeling for Atmospheric Sciences and Geophysical Fluid Dynamics (LASG), the Institute of Atmospheric Physics (IAP) of Chinese Academy of Sciences (Li et al. 2013). FGOALS-g2 consists of the atmosphere components of LASG/IAP [Grid-point Atmospheric Model of IAP LASG version 2 (GAMIL2)] and ocean components of

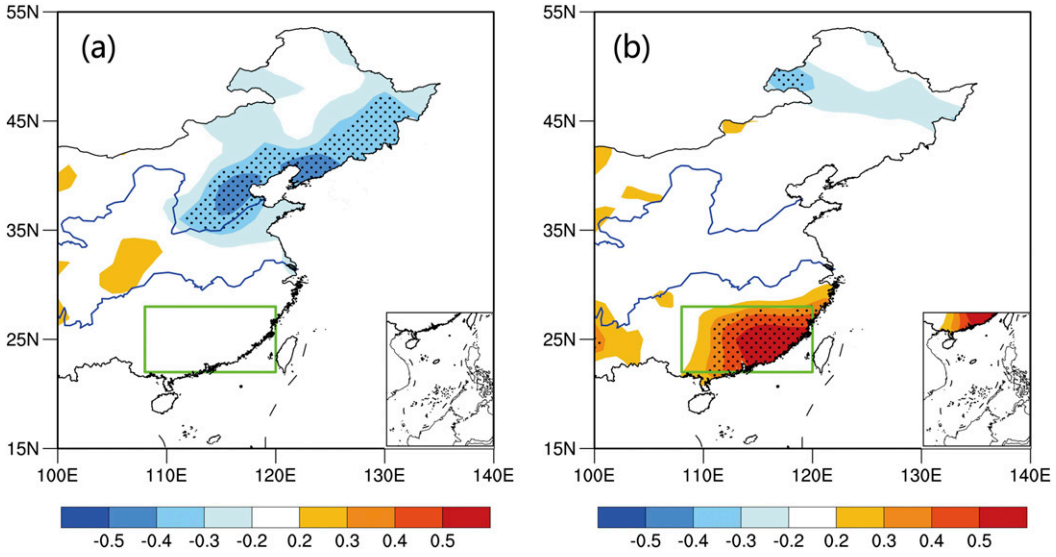

FIG. 3. (a) Correlation maps of the JFM(+1) rainfall anomalies in eastern China with the DJF(0) Niño-3.4 index. (b) As in (a), but with FMA(0)-averaged VMI [with the DJF(0) ENSO signal linearly removed]. Dots show correlations significant above the 95% confidence level.

LASG/IAP Climate System Ocean Model version 2 (LICOM2, with resolutions of about 2.8° × 2.8° and 1° × 1° in the horizontal and 30 and 26 layers in the vertical direction, respectively), coupled with land and sea ice components of the Community Land Surface Model version 3 (CLM3) from the National Center for Atmospheric Research (NCAR) and the improved Community Ice Code version 4 (CICE4) developed by the LASG (CICE4-LASG).

c. *The VM index*

To obtain the VM index (VMI), we apply empirical orthogonal function (EOF) analysis to SSTAs over the North Pacific poleward of 20°N (after removing the monthly mean global averaged SST anomalies) (Fig. 1). The leading EOF mode (EOF1) of SSTAs in the extratropical North Pacific is well known as the Pacific decadal oscillation (PDO) (Mantua et al. 1997; Zhang et al. 1997). The second EOF mode (EOF2) is the VM, which exhibits a northeast–southwest dipole structure in the North Pacific (Bond et al. 2003). The VMI is defined as the principal component (PC2) associated with the EOF2. As previous studies have shown that the VM has maximum variance in boreal spring (FMA) (Ding et al. 2015a,b), we use the FMA-averaged VMI in this study. In addition, as we focus on the interannual connection between the spring VM and the following winter rainfall over SC, interdecadal variability is removed from the time series of FMA VMI and rainfall over SC via fast Fourier transform (FFT) 9-yr high-pass filtering.

d. *Statistical methods*

We employ statistical methods, including EOF analysis, singular value decomposition (SVD), composite analysis, correlation analysis, and linear regression. A two-tailed t test is used to assess statistical significance. Considering the effect of autocorrelations on significance tests for the correlation coefficient between two variables, the number of degrees of freedom for the sample is replaced by the number of effective degrees of freedom (N^{eff}). The formula is as follows (Bretherton et al. 1999):

$$N^{\text{eff}} \approx N\frac{1 - r_x r_y}{1 + r_x r_y}, \tag{1}$$

where N is the sample size, and r_x and r_y represent the lag-one autocorrelations of two time series x and y, respectively.

3. Establishing the relationships between the spring VM and the following winter rainfall over SC

To examine possible relationships between the spring VM and the following winter rainfall over SC, we first calculate the lead–lag correlation between the FMA-averaged VMI and the 3-month averaged rainfall index [RI; defined as the standardized area-averaged rainfall anomalies for SC (22°–28°N, 108°–120°E)]. Here, year 0 refers to the year in which the VM peaks in FMA and year −1 (+1) refers to the preceding (following) year. As seen from Fig. 2a, the correlation coefficient between the FMA VMI and RI exceeds the 95% confidence level starting from November–January [NDJ(0)], and peaks in the following winter [JFM(+1)] when the spring VM leads the SC

TABLE 1. Selected strong positive and negative VM cases and SC rainfall cases during the period 1979–2017.

Case	Years
Positive VM	1982, 1991, 1996, 1997, 2014, 2015
Negative VM	1987, 1988, 1998, 1999, 2001, 2010,2016
Positive SC rainfall	1982, 1984, 1989, 1991, 1994, 1997, 2015
Negative SC rainfall	1983, 1998, 2010, 2013, 2014

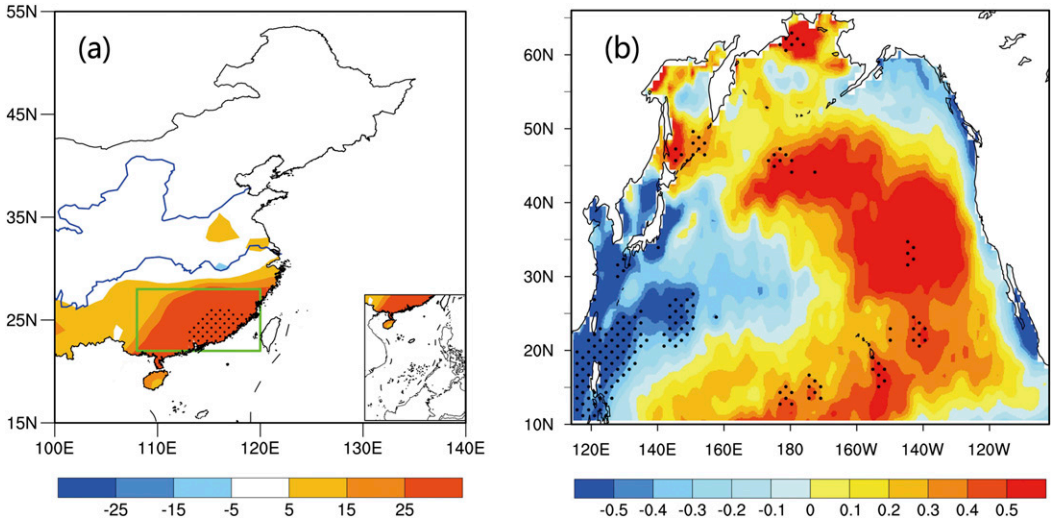

FIG. 4. (a) Composite differences of the JFM(+1) rainfall (unit: mm) in eastern China between positive and negative VM cases. (b) Composite differences of FMA(0) SSTA (unit: °C) over the North Pacific between positive and negative rainfall cases. Stippled areas pass the 95% confidence level.

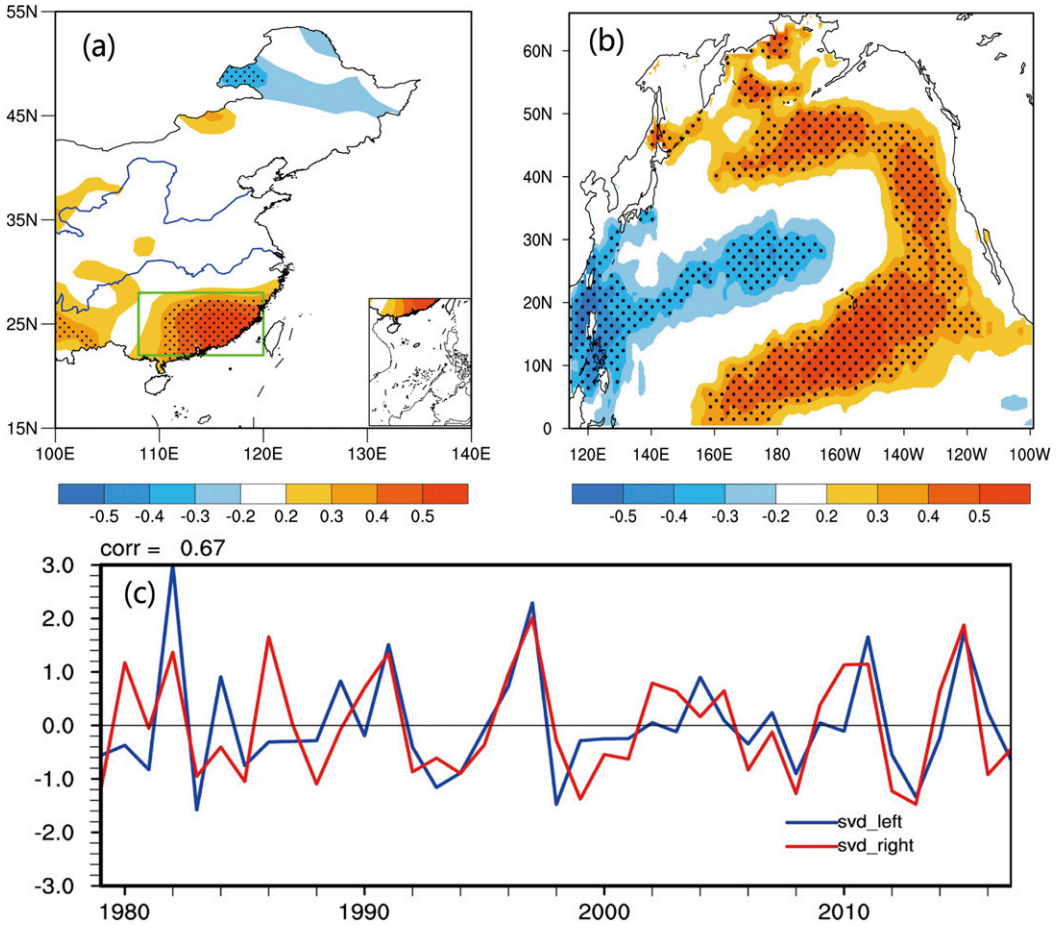

FIG. 5. Spatial distributions of heterogeneous correlation and corresponding expansion coefficients from the first SVD mode of the JFM(+1) rainfall anomalies over eastern China and the FMA(0) SSTA field over the North Pacific. (a) Left heterogeneous correlation. (b) Right heterogeneous correlation. (c) Standardized expansion coefficients of the leading SVD of the JFM(+1) rainfall anomaly field for eastern China (blue line) and the North Pacific FMA(0) SSTA field (red line). In (a) and (b) stippled areas pass the 95% confidence level.

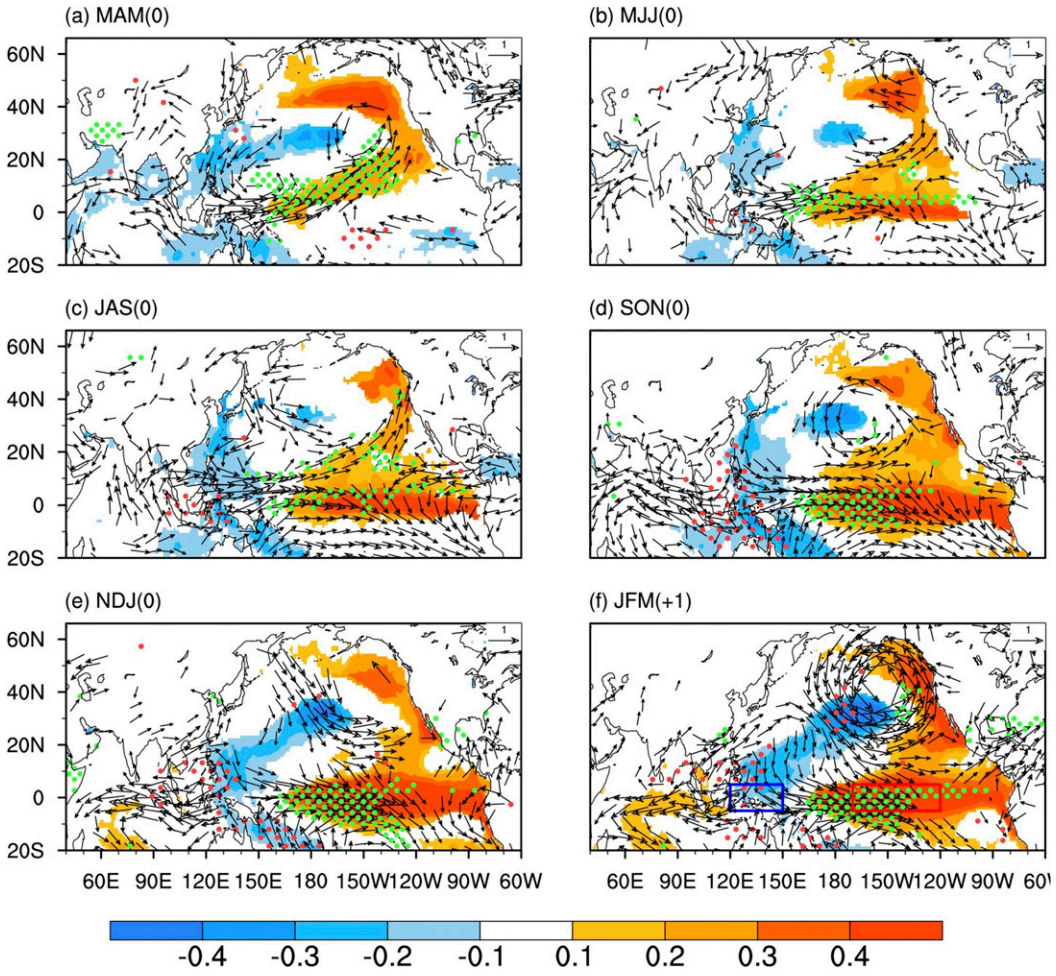

FIG. 6. Regression maps of the 3-month averaged wind vectors at 850 hPa (vectors), SST (shading), and rainfall (stippling) anomalies with respect to FMA(0)-averaged VMI for (a) MAM(0), (b) MJJ (0), (c) JAS(0), (d) SON(0), (e) NDJ(0), and (f) JFM(+1). Green (red) dots denote positive (negative) coefficients. Only areas exceeding the 95% confidence level are displayed.

rainfall by 11 months. The correlation map of the FMA VMI and the following January–March [JFM(+1)] rainfall anomalies in eastern China is shown in Fig. 2b. There are significant positive correlations over SC and relatively weak correlations in other areas. Both the time series of FMA(0) VMI and JFM(+1) RI show significant interannual variability, and the correlation between them is strong ($R = 0.66$, significant at the 99.9% confidence level). These results indicate a significant relationship between spring VM and the following winter rainfall over SC.

Given that ENSO has a notable impact on East Asian climate (Wang et al. 2000), we also calculate the correlation between winter rainfall anomalies in eastern China and the Niño-3.4 index of the previous winter. Significant negative correlations occur in North China and Northeast China while there are weak correlations over SC (Fig. 3a). After removing the previous winter's ENSO signal (represented by the DJF Niño-3.4 index) from the FMA(0) VMI, the correlation pattern of JFM(+1) rainfall anomalies in eastern China related to the FMA(0) VMI does not change from that shown in Fig. 2b (see Fig. 3b). These results indicate a significant positive correlation between the spring VM and the following winter rainfall over SC, and that their relationship is weakly affected by the previous winter's ENSO.

We next use composite analysis to better understand the relationship between the spring VM and the following winter rainfall over SC. We define strong positive (negative) cases of the VM and SC rainfall as having standardized values of the FMA(0) VMI and JFM(+1) RI that are larger (smaller) than 1 (−1) (Table 1). This gives six strong positive and six strong negative VM cases, along with seven strong positive and five strong negative SC rainfall cases. Figure 4a shows the composite difference of the JFM(+1) rainfall in eastern China between positive and negative VM years. Significant positive rainfall anomalies are evident over SC. The composite difference of the FMA(0) SSTAs in the North Pacific between positive and negative rainfall years is displayed in Fig. 4b. The composite difference pattern of SSTAs closely resembles the

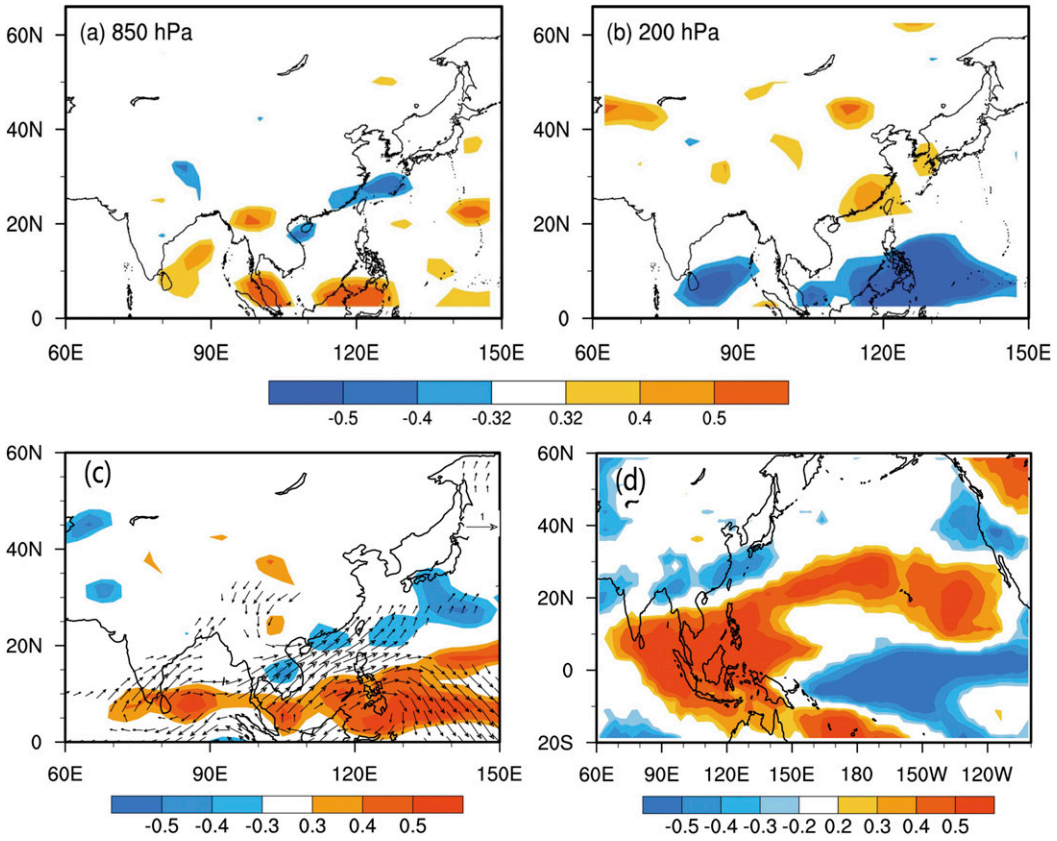

FIG. 7. Correlation maps of FMA(0)-averaged VMI with JFM(+1) divergence over the Northern Hemisphere at (a) 850 and (b) 200 hPa. (c) Correlation map of VMI_FMA with JFM(+1) 850-hPa vertical velocity (shaded) and correlation map of VMI_FMA with JFM(+1) vertically integrated (from the 1000 to 400 hPa) water vapor transport flux (vectors). (d) Correlation map of VMI_FMA with JFM(+1) OLR anomalies. Only areas exceeding the 95% confidence level are displayed in the above plots.

VM, characterized by a warm center in the Pacific poleward of 30°N (near the west coast of North America), and negative SSTAs in the northwest North Pacific (Bond et al. 2003; Ding et al. 2015a).

To further confirm the lagged link between the VM and rainfall over SC, we apply the SVD analysis to the cross-covariance matrix between the FMA(0) SST anomalies in the North Pacific and the JFM(+1) rainfall over eastern China (Fig. 5). The leading mode accounts for 47.7% of the total squared covariance. The correlation coefficient between the corresponding expansion coefficients of the leading mode is 0.67 (Fig. 5c), which is significant at the 99.9% confidence level. Correlations of the expansion coefficients of the FMA(0) North Pacific SSTAs with the FMA(0) VMI and the expansion coefficients of JFM(+1) China rainfall anomalies with JFM(+1) RI are high, with correlation coefficients of 0.78 and 0.92, respectively. This indicates that the SVD time series can be used to represent the spring VM and following winter SC rainfall variability. Figures 5a and 5b show the leading pair of heterogeneous patterns, which are computed by correlating the JFM(+1) rainfall field over eastern China with the SVD leading normalized expansion coefficients of FMA(0) North Pacific SSTAs (Fig. 5a), and correlating the FMA(0) SSTA field with the SVD leading normalized expansion coefficients of the JFM(+1) eastern China rainfall anomalies (Fig. 5b). The FMA(0) North Pacific SSTA field is dominated by a tripole SSTA pattern similar to the VM (Fig. 5b). During the following winter, the rainfall pattern shows strong positive correlations over SC (Fig. 5a). The patterns in Figs. 5a and 5b are consistent with the results from Fig. 4. These patterns indicate that a strong positive VM in late winter and early spring is likely to be followed by increased winter rainfall over SC.

4. Possible mechanisms

As speculated above, there exists an interannual change in the positive connection between the spring VM and the winter rainfall over SC. Previous studies have shown how the VM affects the summer precipitation over the Pacific ITCZ and ENSO through an ocean–atmosphere interaction (Ding et al. 2015a,b). These studies mainly focused on the effects of the VM on tropical climate variability, while the mechanism by which the VM influences the SC rainfall has not been explored. Therefore, in this section, we aim to investigate the underlying mechanism by which the spring VM influences the following

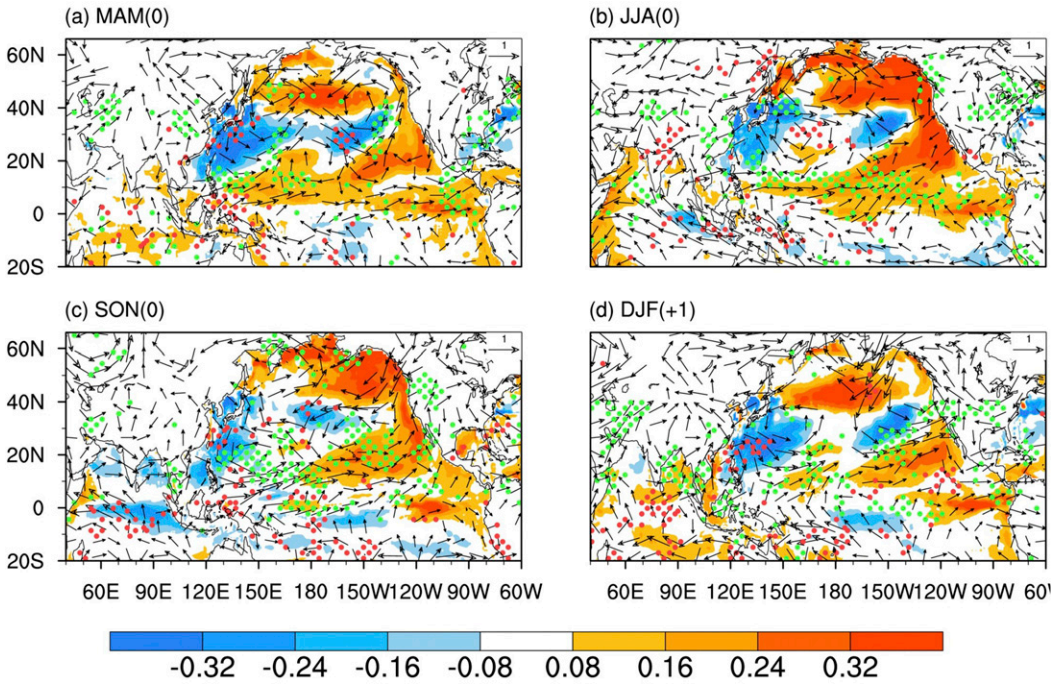

FIG. 8. Composite differences in the seasonal evolution of wind vectors at 850 hPa (vectors), SST (shading), and rainfall (stippling) anomalies between the forcing and control experiments for (a) MAM(0), (b) JJA(0), (c) SON(0), and (d) DJF(+1). Green (red) dots denote positive (negative) coefficients. Only areas exceeding the 90% confidence level are displayed.

winter rainfall over SC by examining the evolutions of the VM-related circulation, SST, and moisture transport.

Figure 6 shows the lagged regressions of 3-month averaged surface wind, SST, and rainfall anomalies with respect to the FMA-averaged VMI. During MAM(0), it shows a tripole-like SSTA pattern over the North Pacific basin, with a negative SSTA band extending from the central North Pacific to the western equatorial Pacific, a positive SSTA band over the central-eastern Bering Sea, and a positive SSTA band associated with the VM extending from the northeast Pacific to the central equatorial Pacific. The significant positive SSTA band associated with the VM extends from the subtropical central-eastern North Pacific toward the central equatorial Pacific, which exhibits a warming over the central equatorial Pacific. This warming, combined with negative SSTAs over the western equatorial Pacific, decreases the zonal SST gradient between the western equatorial Pacific and the central equatorial Pacific, which promotes the development of anomalous westerlies over the equatorial Pacific. Positive SSTAs in the central equatorial Pacific then strengthen via the Bjerknes feedback (Bjerknes 1969), and extend eastward during May–July [MJJ(0)], which is induced by a thermocline feedback (Santoso et al. 2013). At the same time, anomalous westerlies over the central-western equatorial Pacific, in conjunction with anomalous easterlies over the eastern equatorial Pacific, result in convergence and enhanced rainfall over the ITCZ (Ding et al. 2015a). The enhanced rainfall may further favor the low-level convergence through releasing latent heat of condensation to atmosphere. As a result of these positive feedback between SST, wind, and rainfall anomalies, negative SSTAs over the western equatorial Pacific and positive SSTAs over the central-eastern equatorial Pacific further develop and peak during JFM(+1). These surface air–sea coupling processes through which the VM influences ENSO are consistent with those described by previous studies (Ding et al. 2015b, 2018).

In addition to the surface air–sea interaction, it is reported that the VM can induce ENSO through the evolution of subsurface ocean temperature anomalies along the equator. Ding et al. (2015b) pointed out that the subsurface ocean temperature anomalies along the equator related to VM propagate eastward and upward and reach the surface in summer, intensifying the warming in the central-eastern equatorial Pacific and inducing an ENSO in winter.

As El Niño induced by the VM reaches its peak during JFM(+1), the associated SSTA pattern, with negative SSTAs over the western equatorial Pacific and positive SSTAs over the central-eastern equatorial Pacific, initiates an anomalous anticyclone over the WNP (WNPAC) (Fig. 6f). The mechanism by which the ENSO induces the WNPAC has been extensively studied. It is widely believed that the WNPAC is caused by a Rossby wave response to suppressed convective heating over the western tropical Pacific induced by El Niño (Zhang et al. 1996, 1999, 2017; Wang et al. 2000). The correlation map of the spring [FMA(0)] VMI with the following winter [JFM(+1)] outgoing longwave radiation (OLR) exhibits a dipole pattern along the tropical Pacific, characterized by strong

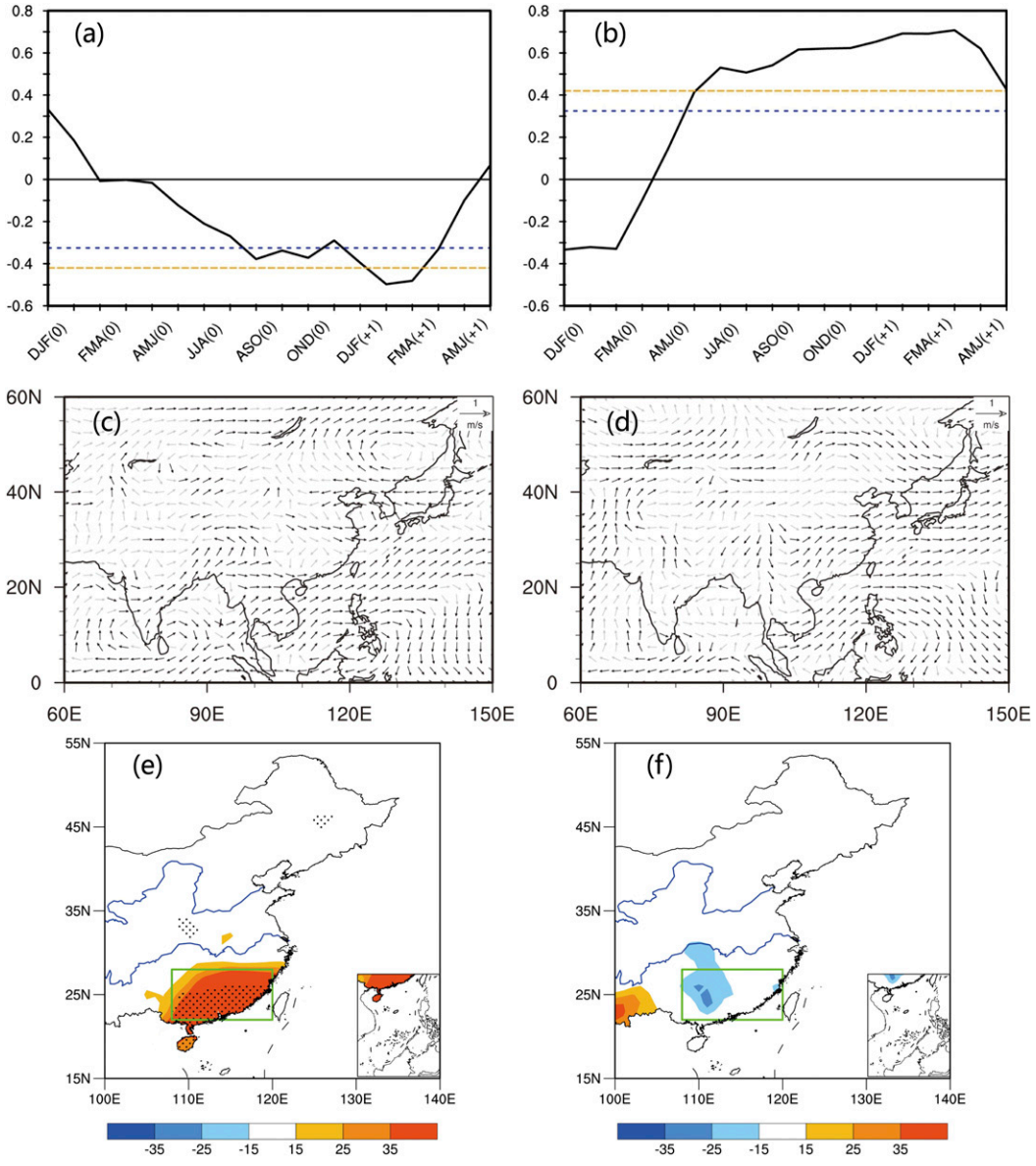

FIG. 9. (a) Lead–lag correlation coefficients between the FMA(0)-averaged VMI and overlapping 3-month averaged WSSTI. (b) As in (a), but with overlapping 3-month averaged Niño-3.4 index. The horizontal dashed lines show the 95% (blue) and 99% (yellow) confidence levels. (c) Composite differences of the JFM(+1) 850-hPa wind anomalies between (positive VM)/El Niño and (negative VM)/La Niña years. (d) Composite differences of the JFM(+1) 850-hPa wind anomalies in eastern China between (no VM event)/El Niño and (no VM event)/La Niña years. Black (gray) vectors are significant (not significant) at the 95% confidence level. (e) Composite differences of the JFM(+1) rainfall in eastern China between (positive VM)/El Niño and (negative VM)/La Niña cases. (f) Composite differences of the JFM(+1) rainfall in eastern China between (positive VM)/(no ENSO event) and (negative VM)/(no ENSO event) cases. Stippled areas pass the 95% confidence level. Note that the small composite sample size may increase uncertainty of the results.

positive correlations over the western tropical Pacific and strong negative correlations over the central and eastern tropical Pacific (Fig. 7d). This indicates that a strong positive VM is followed by an El Niño in the following winter, and then convective cooling anomalies over the western tropical Pacific can trigger an atmospheric Rossby wave response, finally resulting in the generation of the WNPAC.

The northwest branch of the WNPAC consists of anomalous southwesterlies along the southeast coast of East Asia. These southwesterly anomalies contribute to more moisture transport to the southeastern coast of East Asia. This anomalous northeastward moisture transport increases the water vapor supply over SC (Fig. 7c). Meanwhile, the VM-related divergence field is significantly positive at 200 hPa and significantly

TABLE 2. Selected strong positive and negative VM cases associated with positive and negative ENSO cases during the period 1979–2017.

	ENSO		
VM	El Niño	La Niña	No event
Positive	1982, 1991, 1994, 1997, 2002, 2015	—	2014
Negative	—	1988, 1998, 1999, 2010	2001, 2016
No event	1986, 1996, 2009	1984, 2007	—

negative at 850 hPa over SC (Figs. 7a,b), which signifies low-level convergence and high-level divergence over SC. This circulation configuration favors ascending motion (Fig. 7c) and enhanced convection (Fig. 7d) over SC. The combination of northeastward moisture transport and ascending motion leads to increasing rainfall over SC.

In addition to the observational results presented above, we designed forcing and control experiments using the FGOALS-g2 model to further interpret the influences of the VM on the winter rainfall over SC. The difference between the forcing and control experiment is whether to add the VM-related SST anomalies in the North Pacific poleward of 10°N, which is gained from regressions of the FMA SST anomalies onto the concurrent VMI (not shown). The control experiment was forced with the climatological SST, which runs with 23 years of integrations, and the last 12 years were provided for the basic annual mean state. The forcing experiment was forced with the VM-related SST anomalies imposed on the climatological SST, which runs with 18 year of integrations, and the last 12 years were applied to the composite analysis. The composite differences in the seasonal evolutions of SST, precipitation, and surface wind anomalies between the forcing and control experiments are shown in Fig. 8. The results from coupled model sensitivity experiments confirm that the VM-related SST anomalies during spring can extend to the tropics, and subsequently cause El Niño in the following winter. The positive SSTAs over the central-eastern equatorial Pacific and negative SSTAs over the western equatorial Pacific induce the formation of the WNPAC. Finally, positive winter rainfall anomalies occur over SC. These results are almost consistent with those described in observational data (Fig. 6), and further confirm

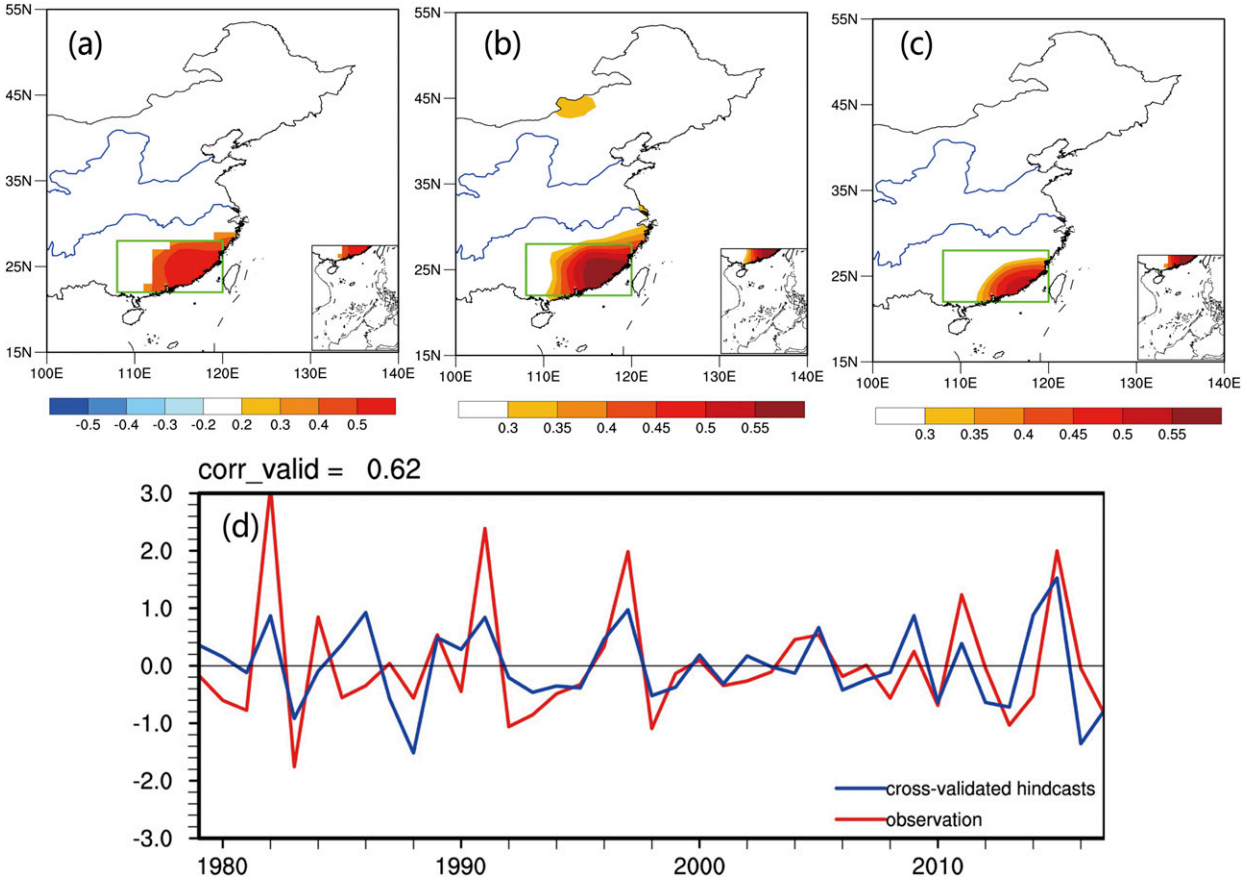

FIG. 10. (a) The distribution of the regression coefficient ε calculated in the empirical prediction model [Eq. (2)]. (b) Correlations between the observed and hindcast JFM(+1) rainfall anomalies obtained from the model [Eq. (2)]. (c) Correlations between observations and fourfold cross-validated hindcasts of JFM(+1) precipitation anomalies. Only areas exceeding the 95% confidence level are displayed in (a)–(c). (d) Time series of observed and fourfold cross-validated hindcast JFM(+1) RI.

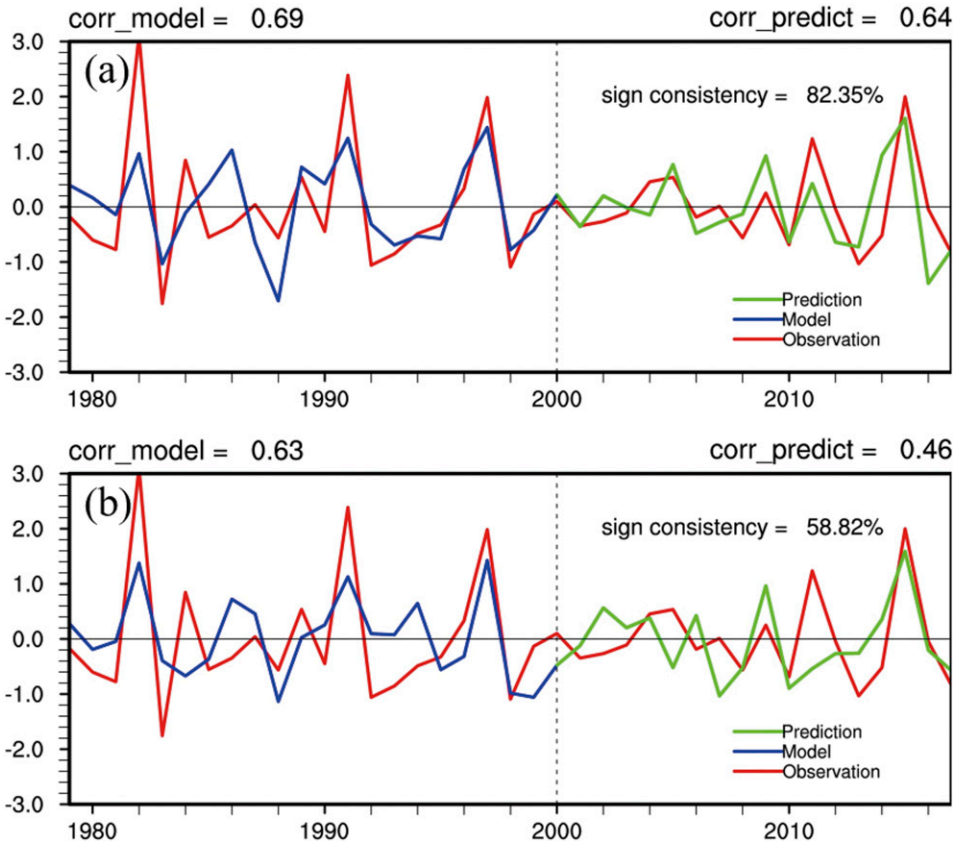

FIG. 11. (a) Time series of observed, modeled, and predicted JFM(+1) RI [with model using FMA(0)-averaged VMI]. Observed annual JFM(+1) RI (red) for 1979 to 2017, model simulated annual JFM RI (blue) for 1979–2000, and predicted annual JFM RI (green) for 2001–17. (b) As in (a), but with a model using the DJF(+1) Niño-3.4 index.

that the VM may have significant impact on the following winter rainfall over SC, and that ENSO and WNPAC play important roles in this process.

The analysis above shows that the VM exerts an essential influence on the winter rainfall over SC. In addition, ENSO and WNPAC play important roles in the link between the VM and rainfall over SC. The cause-and-effect relationships between the spring VM, the following winter ENSO, the following winter WNPAC, and the following winter rainfall over SC are as follows: VM (spring) → ENSO (the following winter) → WNPAC (the following winter) → rainfall over SC (the following winter). These results show that ENSO may act as a bridge through which the North Pacific VM influences the winter rainfall over SC. To further demonstrate this point, we computed the lead–lag correlation between the FMA-averaged VMI and the 3-month running averaged SSTA index over the western equatorial Pacific [WSSTI, defined as the area-averaged SSTAs over the western equatorial Pacific (5°S–5°N, 120°–150°E)] and 3-month running averaged SSTAs over the central-eastern equatorial Pacific (represented by the Niño-3.4 index). The correlation coefficients between the FMA(0)-averaged VMI and overlapping 3-month averaged WSSTI peak at JFM(+1), with a significant negative value of −0.5 (Fig. 9a). The correlation coefficients between the FMA(0)-averaged VMI and overlapping 3-month averaged Niño-3.4 index also peak around JFM(+1), with a significant positive value of 0.6 (Fig. 9b). Simultaneously, correlations of the JFM(+1) WSSTI and the JFM(+1) Niño-3.4 index with the simultaneous RI over SC reach −0.56 and 0.63, respectively (significant above the 99.9% confidence level). These results further show that the spring VM may first affect the ENSO-related SSTAs over the equatorial Pacific during the following winter, which then exert an essential influence on the rainfall over SC. From this perspective, ENSO may act as a bridge for the VM's effects on winter rainfall over SC.

Furthermore, composite analysis is used to elucidate the role of ENSO in the process of the VM's influence on SC rainfall over SC. We defined strong positive (negative) VM/ENSO years as having standardized values of the FMA(0) VMI/DJF(+1) Niño-3.4 index that are larger (smaller) than 1 (−1). Selected strong positive and negative VM cases associated with positive and negative ENSO cases are displayed in Table 2. Figure 9c shows the composite difference of 850-hPa wind anomalies in eastern China between positive VM/El Niño and negative VM/La Niña years. It shows that southwesterly anomalies to the western flank of the WNPAC over SC for only

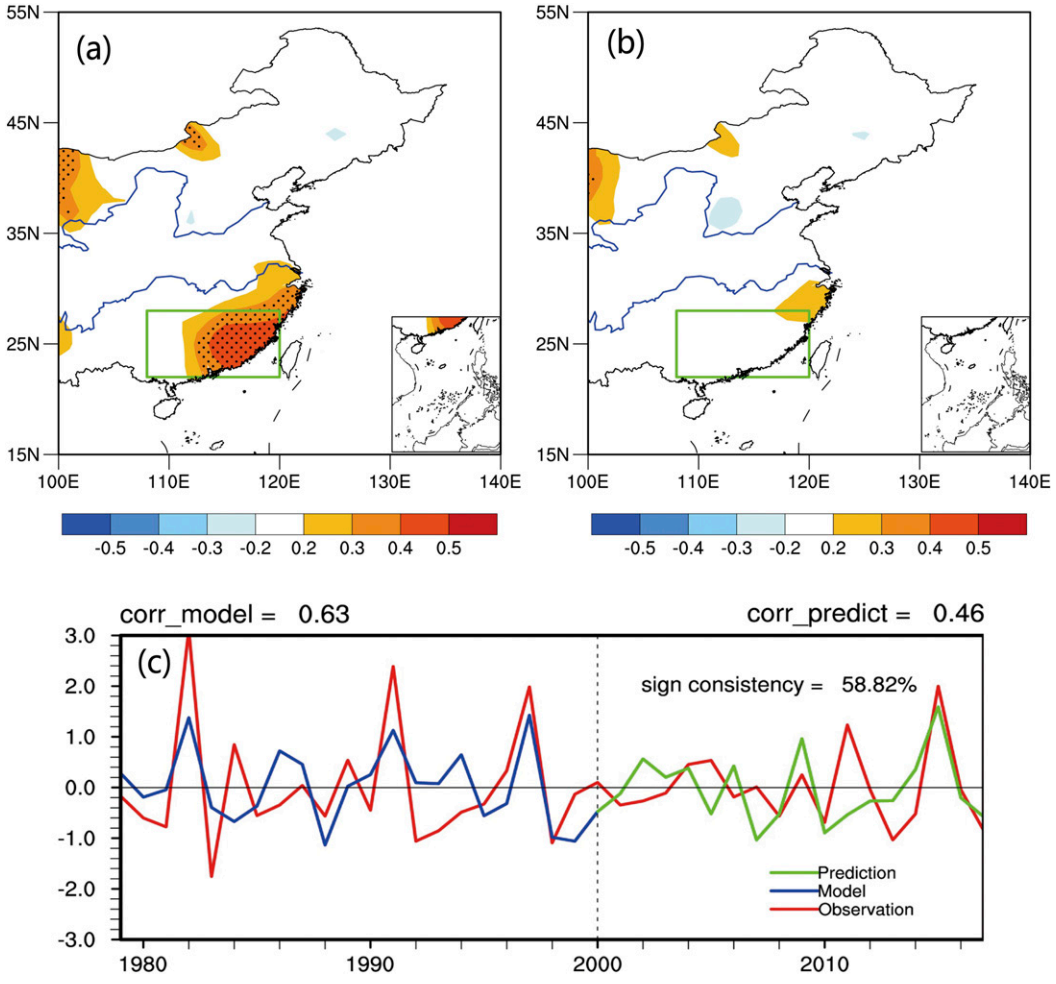

FIG. 12. (a) Correlation map of the JFM(+1) rainfall anomalies in eastern China with the JJA(0) Niño-3.4 index. (b) As in (a), but with the previous VM signal linearly removed from the JJA(0) Niño-3.4 index. In (a) and (b), stippled areas pass the 95% confidence level. (c) Time series of observed, modeled, and predicted JFM RI [with linear regression model using the JJA(0) Niño-3.4 index]. Here, observed annual JFM RI (red) for 1979–2017, model simulated annual JFM RI (blue) for 1979–2000, and predicted annual JFM RI (green) for 2001–17.

VM cases seem to be insignificant compared with the VM co-occurring with ENSO cases (Fig. 9d). As a result, significant positive rainfall anomalies are evident over SC for the VM co-occurring with ENSO cases, while rainfall anomalies over SC become indistinct for only VM cases (Figs. 9e,f). The overall results further confirm that ENSO plays an important role in linking the VM to the rainfall over SC.

5. Prediction

Given that the North Pacific VM has a lagged influence on the winter rainfall over SC, the VM may be used to predict winter SC rainfall about one year in advance. Thus, we establish a simple empirical prediction model to predict the winter [JFM(+1)] SC rainfall by using the spring [FMA(0)] VMI. The model is based on a linear regression method, choosing the spring VMI as the independent variable. The specific formula is as follows:

$$R(t+1) = \varepsilon \times \mathrm{VMI}(t), \tag{2}$$

where VMI refers to the spring VMI at each grid point, and t is time in years. The time series of $R(t+1)$ and VMI(t) have been standardized. A least squares fit gives the regression coefficient ε at each grid point.

Figure 10a shows the spatial distribution of ε based on data for the period 1979–2017. Significant positive ε values exist over SC. The SC winter rainfall hindcasts using the model above are closely related to the observed SC winter rainfall (Fig. 10b). To test the robustness of this model, we conduct the fourfold cross-validation (the original 1979–2017 data are randomly partitioned into four equal-sized subsamples. Of the four subsamples, a single subsample is retained as the validation data for testing the model, and the remaining three subsamples are used to building a linear regression model). The correlation coefficients between observations and cross-validated hindcasts are smaller than those in Fig. 10b, but still high in most regions of SC (Fig. 10c). The time

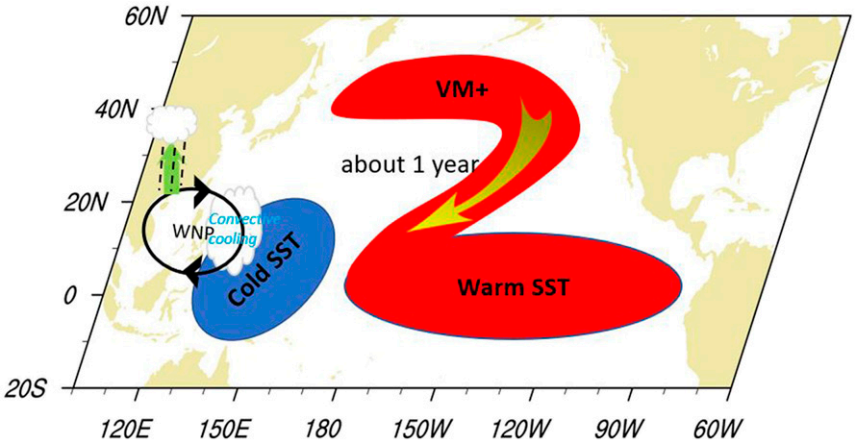

FIG. 13. Schematic diagram explaining how the spring VM affects the following winter rainfall over SC. A strong positive VM during spring induces an El Niño during the following winter via an air–sea interaction. The convective cooling induced by El Niño triggers the formation of WNPAC. The anomalous southwesterlies associated with the WNPAC favor sufficient water vapor supply and anomalous ascending motion over SC, finally resulting in the increase of winter rainfall over SC.

series of cross-validated hindcasted JFM RI and observed JFM RI are displayed in Fig. 10d. The change of cross-validated hindcasts is similar to that of the observations. The high correlation between the cross-validated hindcasts and the observations indicates the relatively good stability of our model.

To further examine the performance of the model, we employ a holdout method, using historical data from 1979 to 2000 to build the model to predict the variation of JFM RI from 2000 to 2017 (Fig. 11a). The correlation between the observed and predicted JFM RI is still high ($R = 0.64$, significant at the 95% confidence level). A high sign consistency rate, with a value of 88.25%, indicates the relatively high prediction skill of this model. In Fig. 11b we show the results for a simple linear regression model constructed using a single DJF(+1) Niño-3.4 index to predict JFM RI; both the correlation coefficient between the observed and predicted JFM RI and sign consistency rate are lower than those in Fig. 11a. Figures 12a and 12b show correlation maps of the JFM(+1) rainfall anomalies in eastern China with the JJA(0) Niño-3.4 index before and after removing the previous VM signal [represented by the FMA(0) VMI] from the JJA(0) Niño-3.4 index. The correlation coefficients over SC are drastically reduced after removing the previous VM signal, indicating that the relationship between ENSO and the following winter rainfall over SC is significantly affected by the VM. The prediction skill of the JJA(0) Niño-3.4 index for JFM(+1) rainfall is even lower (with a smaller correlation coefficient between the observed and predicted JFM RI and less sign consistency) (Fig. 12c). These results indicate that although ENSO is the strongest signal of the East Asian climate (Yuan and Yang 2012), the predictive ability of the VM is better than that of ENSO in forecasting winter rainfall over SC. Therefore, the VM can be used to predict the following winter rainfall over SC effectively about one year in advance.

6. Summary and discussion

This study has focused on the relationships between the North Pacific VM and rainfall over SC. Results show that the VM, which peaks in spring, exerts a lagged influence on the following winter SC rainfall. When the spring VM is positive, the following winter rainfall over SC tends to be greater than normal.

The thermodynamic mechanism for the effect of the VM on the following winter SC rainfall is summarized in Fig. 13. When the VM peaks in spring, significant positive SSTAs associated with the VM extend from the subtropical central-eastern North Pacific to the equator. Positive SSTAs over the central equatorial Pacific develop via a Bjerknes positive feedback and extend eastward, resulting in the formation of an El Niño, with strong positive SSTAs over the central-eastern equatorial Pacific and strong negative SSTAs over the western equatorial Pacific during the following winter. The convective cooling anomalies over the western tropical Pacific induced by El Niño trigger an atmospheric Rossby wave response, and generate the WNPAC. The resulting anomalous southwesterlies along the southeast coast of East Asia, which is the northwestern branch of the WNPAC, largely increase moisture from the Indian Ocean and SCS, and thus sufficient water vapor supply and anomalous ascending motion occur over SC and rainfall over SC increases.

A simple empirical prediction model is constructed to predict winter rainfall over SC using the VM. The predicted winter rainfall over SC by the model is similar to the observation. High correlation and sign consistency between the hindcasted and observed RI indicates that the VM can be applied to simulate the variation of winter rainfall over SC. Compared to ENSO, the VM has relatively higher prediction skill in predicting winter rainfall over SC.

In conclusion, it is clear that the VM can act as an effective predictor of winter rainfall over SC about one year in advance. However, to predict the variations of SC rainfall more accurately, it may not be sufficient to only consider the contribution of the VM. Further research is required to find more predictors of winter rainfall over SC. And how to consider the joint prediction of multiple factors is an issue that needs to be addressed.

Acknowledgments. The authors are grateful for the very constructive comments of three reviewers. This work was jointly supported by the National Natural Science Foundation of China (Grants 41790474 and 41975070) and the 973 project of China (2016YFA0601801).

REFERENCES

Bjerknes, J., 1969: Atmospheric teleconnections from the equatorial Pacific. *Mon. Wea. Rev.*, **97**, 163–172, https://doi.org/10.1175/1520-0493(1969)097<0163:ATFTEP>2.3.CO;2.

Bond, N. A., J. E. Overland, M. Spillane, and P. Stabeno, 2003: Recent shifts in the state of the North Pacific. *Geophys. Res. Lett.*, **30**, 2183, https://doi.org/10.1029/2003GL018597.

Bretherton, C. S., M. Widmann, V. P. Dymnikov, J. M. Wallace, and I. Bladé, 1999: The effective number of spatial degrees of freedom of a time-varying field. *J. Climate*, **12**, 1990–2009, https://doi.org/10.1175/1520-0442(1999)012<1990:TENOSD>2.0.CO;2.

Chan, J. C. L., and W. Zhou, 2005: PDO, ENSO and the early summer monsoon rainfall over South China. *Geophys. Res. Lett.*, **32**, L08810, https://doi.org/10.1029/2004GL022015.

——, Y. Liu, K. C. Chow, Y. Ding, W. K. M. Lau, and K. L. Chan, 2004: Design of a regional climate model for the simulation of South China summer monsoon rainfall. *J. Meteor. Soc. Japan*, **82**, 1645–1665, https://doi.org/10.2151/jmsj.82.1645.

Chang, X., B. Wang, Y. Yan, Y. Hao, and M. Zhang, 2019: Characterizing effects of monsoons and climate teleconnections on precipitation in China using wavelet coherence and global coherence. *Climate Dyn.*, **52**, 5213–5228, https://doi.org/10.1007/s00382-018-4439-1.

Chen, J., Z. Wen, R. Wu, Z. Chen, and P. Zhao, 2014: Interdecadal changes in the relationship between southern China winter–spring precipitation and ENSO. *Climate Dyn.*, **43**, 1327–1338, https://doi.org/10.1007/s00382-013-1947-x.

Chen, T. C., W. R. Huang, and M. C. Yen, 2011: Interannual variation of the late spring–early summer monsoon rainfall in the northern part of the South China Sea. *J. Climate*, **24**, 4295–4313, https://doi.org/10.1175/2011JCLI3930.1.

Ding, R., J. Li, Y. H. Tseng, and C. Ruan, 2015a: Influence of the North Pacific Victoria mode on the Pacific ITCZ summer precipitation. *J. Geophys. Res. Atmos.*, **120**, 964–979, https://doi.org/10.1002/2014JD022364.

——, ——, ——, S. Cheng, and Y. Guo, 2015b: The Victoria mode in the North Pacific linking extratropical sea level pressure variations to ENSO. *J. Geophys. Res. Atmos.*, **120**, 27–45, https://doi.org/10.1002/2014JD022221.

——, ——, Y. Tseng, L. Li, C. Sun, and F. Xie, 2018: Influences of the North Pacific Victoria mode on the South China Sea summer monsoon. *Atmosphere*, **9**, 229, https://doi.org/10.3390/atmos9060229.

Duan, W., L. Song, L. Yun, and J. Mao, 2013: Modulation of PDO on the predictability of the interannual variability of early summer rainfall over south China. *J. Geophys. Res. Atmos.*, **118**, 13 008–13 021, https://doi.org/10.1002/2013JD019862.

Gao, R., R. Zhang, M. Wen, and T. Li, 2019: Interdecadal changes in the asymmetric impacts of ENSO on wintertime rainfall over China and atmospheric circulations over western North Pacific. *Climate Dyn.*, **52**, 7525–7536, https://doi.org/10.1007/s00382-018-4282-4.

Ge, J., X. Jia, and H. Lin, 2016: The interdecadal change of the leading mode of the winter precipitation over China. *Climate Dyn.*, **47**, 2397–2411, https://doi.org/10.1007/s00382-015-2970-x.

Huang, W., X. Yang, M. Li, X. Zhang, M. Wang, S. Dai, and J. Ma, 2010: Evolution characteristics of seasonal drought in the south of China during the past 58 years based on standardized precipitation index (in Chinese). *Trans. Chin. Soc. Agric. Eng.*, **26**, 50–59, https://10.3969/j.issn.1002-6819.2010.07.009.

Jia, X., and J. Ge, 2017: Interdecadal changes in the relationship between ENSO, EAWM, and the wintertime precipitation over China at the end of the twentieth century. *J. Climate*, **30**, 1923–1937, https://doi.org/10.1175/JCLI-D-16-0422.1.

Kanamitsu, M., W. Ebisuzaki, J. Woollen, S.-K. Yang, J. J. Hnilo, M. Fiorino, and G. L. Potter, 2002: NCEP–DOE AMIP-II Reanalysis (R-2). *Bull. Amer. Meteor. Soc.*, **83**, 1631–1644, https://doi.org/10.1175/BAMS-83-11-1631.

Li, C., and H. Ma, 2012: Relationship between ENSO and winter rainfall over Southeast China and its decadal variability. *Adv. Atmos. Sci.*, **29**, 1129–1141, https://doi.org/10.1007/s00376-012-1248-z.

——, and J. Sun, 2015: Role of the subtropical westerly jet waveguide in a southern China heavy rainstorm in December 2013. *Adv. Atmos. Sci.*, **32**, 601–612, https://doi.org/10.1007/s00376-014-4099-y.

——, and T. Zhao, 2019: Seasonal responses of precipitation in China to El Niño and positive Indian Ocean dipole modes. *Atmosphere*, **10**, 372, https://doi.org/10.3390/atmos10070372.

Li, L., and Coauthors, 2013: The Flexible Global Ocean–Atmosphere–Land System model, grid-point version 2: FGOALS-g2. *Adv. Atmos. Sci.*, **30**, 543–560, https://doi.org/10.1007/s00376-012-2140-6.

Lin, Z., and R. Lu, 2009: The ENSO's effect on eastern China rainfall in the following early summer. *Adv. Atmos. Sci.*, **26**, 333–342, https://doi.org/10.1007/s00376-009-0333-4.

Lou, M., C. Li, S. Hao, and J. Liu, 2017: Variations of winter precipitation over southeastern China in association with the North Atlantic Oscillation. *J. Meteor. Res.*, **31**, 476–489, https://doi.org/10.1007/s13351-017-6103-9.

Lu, B., A. A. Scaife, N. Dunstone, D. Smith, H.-L. Ren, Y. Liu, and R. Eade, 2017: Skillful seasonal predictions of winter precipitation over southern China. *Environ. Res. Lett.*, **12**, 074021, https://doi.org/10.1088/1748-9326/aa739a.

Mantua, N. J., S. R. Hare, Y. Zhang, J. M. Wallace, and R. C. Francis, 1997: A Pacific interdecadal climate oscillation with impacts on salmon production. *Bull. Amer. Meteor. Soc.*, **78**, 1069–1080, https://doi.org/10.1175/1520-0477(1997)078<1069:APICOW>2.0.CO;2.

Mao, J., J. C. L. Chan, and G. Wu, 2011: Interannual variations of early summer monsoon rainfall over South China under different PDO backgrounds. *Int. J. Climatol.*, **31**, 847–862, https://doi.org/10.1002/joc.2129.

Peng, J., 2012: Influence of the sea surface temperature in the eastern Indian Ocean on the wintertime rainfall in the southern part of China (in Chinese). *Climate Environ. Res.*, **17**, 327–338.

Pu, X., Q. Chen, Q. Zhong, R. Ding, and T. Liu, 2019: Influence of the North Pacific Victoria mode on western North Pacific tropical cyclone genesis. *Climate Dyn.*, **52**, 245–246, https://doi.org/10.1007/s00382-018-4129-z.

Rayner, N., D. E. Parker, E. B. Horton, C. K. Folland, L. V. Alexander, D. P. Rowell, E. C. Kent, and A. Kaplan, 2003: Global analyses of sea surface temperature, sea ice, and night marine air temperature since the late nineteenth century. *J. Geophy. Res.*, **108**, 4407, https://doi.org/10.1029/2002JD002670.

Santoso, A., S. McGregor, F.-F. Jin, W. Cai, M. H. England, S.-I. An, M. J. McPhaden, and E. Guilyardi, 2013: Late-twentieth-century emergence of the El Niño propagation asymmetry and future projections. *Nature*, **504**, 126–130, https://doi.org/10.1038/nature12683.

Sui, Y., D. Jiang, and Z. Tian, 2013: Latest update of the climatology and changes in the seasonal distribution of precipitation over China. *Theor. Appl. Climatol.*, **113**, 599–610, https://doi.org/10.1007/s00704-012-0810-z.

Wang, B., R. Wu, and X. Fu, 2000: Pacific–East Asian teleconnection: How does ENSO affect East Asian climate? *J. Climate*, **13**,

1517–1536, https://doi.org/10.1175/1520-0442(2000)013<1517:PEATHD>2.0.CO;2.

Wu, B., T. Li, and T. Zhou, 2010: Asymmetry of atmospheric circulation anomalies over the western North Pacific between El Niño and La Niña. *J. Climate*, **23**, 4807–4822, https://doi.org/10.1175/2010JCLI3222.1.

——, T. Zhou, and T. Li, 2017: Atmospheric dynamic and thermodynamic processes driving the western North Pacific anomalous anticyclone during El Niño. Part I: Maintenance mechanisms. *J. Climate*, **30**, 9621–9635, https://doi.org/10.1175/JCLI-D-16-0489.1.

Wu, B. Y., and J. Wang, 2002: Winter Arctic oscillation, Siberian high and East Asian winter monsoon. *Geophys. Res. Lett.*, **29**, 1897, https://doi.org/10.1029/2002GL015373.

Wu, R., Z. Z. Hu, and B. P. Kirtman, 2003: Evolution of ENSO-related rainfall anomalies in East Asia. *J. Climate*, **16**, 3742–3758, https://doi.org/10.1175/1520-0442(2003)016<3742:EOERAI>2.0.CO;2.

Xie, S.-P., K. Hu, J. Hafner, H. Tokinaga, Y. Du, G. Huang, and T. Sampe, 2009: Indian Ocean capacitor effect on Indo–western Pacific climate during the summer following El Niño. *J. Climate*, **22**, 730–747, https://doi.org/10.1175/2008JCLI2544.1.

Yi, S., F. Zheng, and H. Luo, 2019: ENSO combination mode and its influence on seasonal precipitation over southern China simulated by ECHAM5/MPI-OM. *Atmos. Oceanic Sci. Lett.*, **12**, 184–191, https://doi.org/10.1080/16742834.2019.1589366.

Yim, S. Y., B. Wang, and W. Xing, 2014: Prediction of early summer rainfall over South China by a physical–empirical model. *Climate Dyn.*, **43**, 1883–1891, https://doi.org/10.1007/s00382-013-2014-3.

Yuan, C., and M. Yang, 2020: Interannual variations in summer precipitation in Southwest China: Anomalies in moisture transport and the role of the tropical Atlantic. *J. Climate*, **33**, 5993–6007, https://doi.org/10.1175/JCLI-D-19-0809.1.

Yuan, Y., and S. Yang, 2012: Impacts of different types of El Niño on the East Asian climate: Focus on ENSO cycles. *J. Climate*, **25**, 7702–7722, https://doi.org/10.1175/JCLI-D-11-00576.1.

Zhang, L., K. Fraedrich, X. Zhu, F. Sielmann, and X. Zhi, 2015: Interannual variability of winter precipitation in Southeast China. *Theor. Appl. Climatol.*, **119**, 229–238, https://doi.org/10.1007/s00704-014-1111-5.

Zhang, R., and A. Sumi, 2002: Moisture circulation over East Asia during El Niño episode in northern winter, spring and autumn. *J. Meteor. Soc. Japan*, **80**, 213–227, https://doi.org/10.2151/jmsj.80.213.

——, ——, and M. Kimoto, 1996: Impact of El Niño on the East Asian monsoon. *J. Meteor. Soc. Japan*, **74**, 49–62, https://doi.org/10.2151/jmsj1965.74.1_49.

——, ——, and ——, 1999: A diagnostic study of the impact of El Niño on the precipitation in China. *Adv. Atmos. Sci.*, **16**, 229–241, https://doi.org/10.1007/BF02973084.

——, Q. Min, and J. Su, 2017: Impact of El Niño on atmospheric circulations over East Asia and rainfall in China: Role of the anomalous western North Pacific anticyclone. *Sci. China Earth Sci.*, **60**, 1124–1132, https://doi.org/10.1007/s11430-016-9026-x.

Zhang, Y., J. M. Wallace, and D. S. Battisti, 1997: ENSO-like interdecadal variability: 1900–93. *J. Climate*, **10**, 1004–1020, https://doi.org/10.1175/1520-0442(1997)010<1004:ELIV>2.0.CO;2.

Zhou, B., and H. Wang, 2006: Relationship between the boreal spring Hadley circulation and the summer precipitation in the Yangtze River valley. *J. Geophy. Res.*, **111**, D16109, https://doi.org/10.1029/2005JD007006.

Zhou, L.-T., 2011: Impact of East Asian winter monsoon on rainfall over southeastern China and its dynamical process. *Int. J. Climatol.*, **31**, 677–686, https://doi.org/10.1002/joc.2101.

——, and R. Wu, 2010: Respective impacts of the East Asian winter monsoon and ENSO on winter rainfall in China. *J. Geophys. Res.*, **115**, D02107, https://doi.org/10.1029/2009JD012502.

——, C.-Y. Tam, W. Zhou, and J. C. L. Chan, 2010: Influence of South China Sea SST and the ENSO on winter rainfall over South China. *Adv. Atmos. Sci.*, **27**, 832–844, https://doi.org/10.1007/s00376-009-9102-7.

Zhou, W., J. C. L. Chan, W. Chen, J. Ling, J. G. Pinto, and Y. Shao, 2009: Synoptic-scale controls of persistent low temperature and icy weather over Southern China in January 2008. *Mon. Wea. Rev.*, **137**, 3978–3991, https://doi.org/10.1175/2009MWR2952.1.